Liquid Crystals
Publication details, including instructions for authors and subscription information:
http://www.informaworld.com/smpp/title~content=t713926090

Dynamics of the acousto-optic effect in a nematic liquid crystal

V. A. Greanya[a]; A. P. Malanoski[a]; B. T. Weslowski[a]; M. S. Spector[a]; J. V. Selinger[a]
[a] Center for Bio/Molecular Science and Engineering, Naval Research Laboratory, Washington, DC 20375

To cite this Article Greanya, V. A. , Malanoski, A. P. , Weslowski, B. T. , Spector, M. S. and Selinger, J. V.(2005) 'Dynamics of the acousto-optic effect in a nematic liquid crystal', Liquid Crystals, 32: 7, 933 — 941
To link to this Article: DOI: 10.1080/02678290500191113
URL: http://dx.doi.org/10.1080/02678290500191113

Liquid Crystals, Vol. 32, No. 7, July 2005, 933–941

Dynamics of the acousto-optic effect in a nematic liquid crystal

V.A. GREANYA, A.P. MALANOSKI, B.T. WESLOWSKI, M.S. SPECTOR and J.V. SELINGER*
Center for Bio/Molecular Science and Engineering, Naval Research Laboratory, Code 6900, 4555 Overlook Avenue, SW, Washington, DC 20375, USA

(*Received 14 November 2004; in final form 5 April 2005; accepted 21 April 2005*)

In a nematic liquid crystal cell, the application of an ultrasonic wave induces a rotation of the director, leading to a change in the optical transmission through the cell. In this study, we investigate the dynamic response of the optical intensity after the ultrasonic wave is switched on or off. Our experiments show that the optical intensity follows a double-exponential function of time, indicating that the system has two relaxation modes with widely different time scales. The fast mode has an amplitude and time scale qualitatively consistent with the dynamics of the Fréedericksz transition, but the slow mode shows novel behaviour associated with the acousto-optic effect.

1. Introduction

When an ultrasonic wave is applied to a nematic liquid crystal cell, it interacts with the orientational order, leading to a realignment of the liquid crystal molecules, and hence to a change in the optical intensity transmitted through the cell [1–3]. This acousto-optic effect can be exploited to visualize variations in the intensity of an ultrasonic wave. It is already being used for non-destructive testing of materials, and it has further potential applications in medical diagnostics and underwater imaging [4–6].

In recent papers, we have investigated the steady state acousto-optic effect in nematic liquid crystals both theoretically and experimentally [7–9]. On the theoretical side, we have shown that the acousto-optic effect can be understood in terms of an effective aligning potential, which tends to orient the liquid crystal director perpendicular to the acoustic wave vector, along the wave fronts. On the experimental side, we have found that the acousto-optic effect is quite sensitive to several physical parameters, including the intensity and angle of the incident ultrasonic wave and the geometry of the liquid crystal cell, and this dependence is consistent with theoretical predictions. In addition, Bonetto *et al.* have recently studied the acoustic realignment of nematic liquid crystals using NMR techniques, and have explained the results in terms of the same type of theory [10–12].

*Corresponding author.
Email: jvs@lci.kent.edu and spectom@onr.navy.mil

In this paper, we extend our earlier steady state investigation to consider the dynamic response of a nematic liquid crystal to an ultrasonic wave. This issue is important for both basic science and applications. For basic science, the comparison of the liquid crystal response to an ultrasonic wave with the response to an electric or magnetic field in the Fréedericksz transition [13, 14] is of interest. In the Fréedericksz transition, the liquid crystal orientation relaxes exponentially toward the equilibrium profile; does the same exponential relaxation occur in the acousto-optic effect? For applications, how does the optical intensity change when an ultrasonic wave is switched on or off, and how does this dynamic process affect the function of imaging devices?

To address this dynamic issue, we measure the optical intensity as a function of time after an ultrasonic wave is switched on or off, for several different values of the initial or final acoustic intensity. We compare the experimental data with predictions of a continuum elastic theory, similar to the dynamic theory of the Fréedericksz transition. Surprisingly, we find that the data for optical intensity vs. time do not follow a simple, single-exponential curve. Rather, a double-exponential function is required to fit the data. This result indicates that the liquid crystal has two distinct relaxation modes with very different time scales. The fast mode is qualitatively consistent with theoretical predictions, in the dependence of its amplitude and relaxation time on acoustic intensity. However, the slow mode seems to be new behaviour associated with the acousto-optic effect in contrast with the electric or magnetic Fréedericksz transition.

Liquid Crystals
ISSN 0267-8292 print/ISSN 1366-5855 online © 2005 Taylor & Francis
http://www.tandf.co.uk/journals
DOI: 10.1080/02678290500191113

2. Theory

In this section, we present a model for the acousto-optic effect. We first review the theory for the steady state behaviour, following the argument in our previous papers [7, 9], and then generalize this theory to predict the dynamic response.

Consider an acoustic wave passing through a nematic liquid crystal, as shown in figure 1. The local orientation of the liquid crystal is specified by the director **n**, which is at an angle β with respect to the z-axis. The acoustic wave has the wave vector **k**, at an angle θ with respect to the z-axis. When the acoustic wave is off, the liquid crystal orientation is determined by the homeotropic cell walls, so that $\beta=0$. When the acoustic wave is switched on, the liquid crystal molecules in the cell interior rotate away from the wave vector **k**, toward alignment with the wave fronts.

To determine the extent of realignment, we must calculate the aligning potential of the acoustic wave on the liquid crystal. In general, the interaction between the director **n** and gradients in the density ρ can be written as

$$V_{\text{int}} = u_1 n_i n_j (\partial_i \partial_j \rho) + u_2 n_i n_j (\partial_i \rho)(\partial_j \rho) \tag{1}$$

where u_1 and u_2 are phenomenological coupling coefficients which characterize the particular liquid crystalline material. An acoustic wave leads to a sinusoidal modulation of the density, which has the form

$$\rho(\mathbf{r}, t) = \rho_0 + \Delta\rho \sin(\mathbf{k}\cdot\mathbf{r} - \omega t). \tag{2}$$

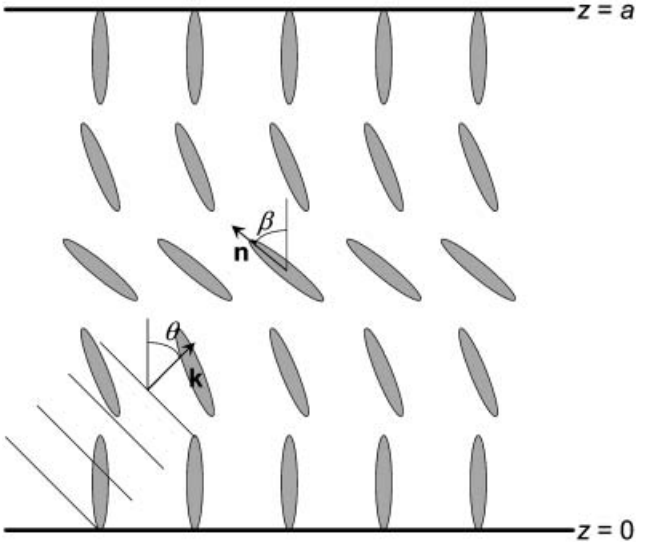

Figure 1. Schematic view of the director orientation profile $\beta(z)$ across a liquid crystal cell, when an ultrasonic wave passes through the liquid crystal at an angle θ.

When we insert this expression for ρ into V_{int}, and average over many cycles of the rapidly oscillating wave, the first term vanishes and the second term becomes

$$\langle V_{\text{int}} \rangle = \frac{1}{2} u_2 (\Delta\rho)^2 (\mathbf{k}\cdot\mathbf{n})^2. \tag{3}$$

The acoustic intensity I is related to the density variation by $I = v^3 (\Delta\rho)^2/(2\rho_0)$, where v is the sound velocity. Hence, the time-averaged interaction potential can be expressed as

$$\langle V_{\text{int}} \rangle = \frac{u_2 \rho_0 k^2 I}{v^3} \cos^2(\beta - \theta) \tag{4}$$

where $(\beta-\theta)$ is the angle between the director and the acoustic wave vector.

Realigning the director in the interior of the cell requires a bend distortion, as shown in figure 1. We can combine the elastic energy cost of this distortion with the acoustic aligning potential to obtain the total free energy per unit area,

$$F = \int_0^a \mathrm{d}z \left[\frac{1}{2} K_3 \left(\frac{\partial \beta}{\partial z} \right)^2 + \frac{u_2 \rho_0 k^2 I}{v^3} \cos^2(\beta - \theta) \right] \tag{5}$$

where a is the cell thickness. A general expression for $\beta(z, t)$, which satisfies the boundary conditions $\beta(0, t) = \beta(a, t) = 0$, is the Fourier series

$$\beta(z, t) = \sum_{j=1}^{\infty} \beta_j(t) \sin \frac{j\pi z}{a}. \tag{6}$$

We can minimize F over the coefficients of this Fourier series. All of the even coefficients vanish by symmetry, while the odd coefficients are non-zero. Each odd coefficient β_j can be expanded in a power series for low acoustic intensity, which gives the steady state solution

$$\beta_j^{\text{eq}} = -\frac{4a^2 u_2 \rho_0 k^2 I \sin 2\theta}{\pi^3 j^3 K_3 v^3} - \frac{4a^4 u_2^2 \rho_0^2 k^4 I^2 \sin 4\theta}{\pi^5 j^5 K_3^2 v^6} - \cdots. \tag{7}$$

We can compare our predictions for the steady state acousto-optic effect with the classical Fréedericksz transition in nematic liquid crystals. In a Fréedericksz experiment, a liquid crystal with a negative dielectric (or diamagnetic) anisotropy is initially aligned along the z-axis, perpendicular to the cell walls, and then an electric (or magnetic) field is applied along the same axis. In that case, the molecules may tilt in any direction away from the z-axis; all tilt directions have equal free energy. Hence, the molecules remain vertical up to a critical threshold field, at which point the system undergoes a spontaneous symmetry-breaking transition and the molecules tilt in a random direction. By contrast,

in our acousto-optic experiment, the acoustic wave passes through the liquid crystal at an angle θ. This acoustic angle breaks the symmetry around the z-axis, and favours a particular orientation for the molecular tilt. As a result, there is no threshold field and no symmetry-breaking transition. Rather, the molecular tilt scales linearly with applied acoustic intensity I, in the limit of low I.

Now that we have derived the steady state acousto-optic effect, we can predict the dynamic response of the liquid crystal to a change in acoustic intensity. The equation of motion for the director angle is

$$\gamma_1 \frac{\partial \beta(z,\, t)}{\partial t} = -\frac{\delta F}{\delta \beta(z,\, t)} \tag{8}$$

where γ_1 is the rotational viscosity of the liquid crystalline material. With the free energy of equation (5), we obtain

$$\gamma_1 \frac{\partial \beta(z,\, t)}{\partial t} = K_3 \frac{\partial^2 \beta(z,\, t)}{\partial z^2} + \frac{u_2 \rho_0 k^2 I}{2v^3} \sin 2(\beta - \theta). \tag{9}$$

As in the steady state case, we can write $\beta(z,\, t)$ as a Fourier series, and expand the equation of motion in a power series for low acoustic intensity. The equation for each Fourier mode j then becomes

$$\gamma_1 \frac{\partial \beta_j(t)}{\partial t} = -\left(\frac{K_3 j^2 \pi^2}{a^2} - \frac{u_2 \rho_0 k^2 I \cos 2\theta}{v^3}\right)\left[\beta_j(t) - \beta_j^{\mathrm{eq}}\right] \tag{10}$$

where β_j^{eq} is the steady state solution found above.

We can solve this equation of motion for the two specific cases of switching the ultrasonic wave on or off. First, suppose that the ultrasonic wave is suddenly switched on from zero to an acoustic intensity of I. The solution for each Fourier mode j is therefore

$$\beta_j(t) = \beta_j^{\mathrm{eq}}\left[1 - \exp\left(-t/\tau_j^{\mathrm{ON}}\right)\right] \tag{11}$$

with the on-time

$$\tau_j^{\mathrm{ON}} = \frac{\gamma_1 a^2}{K_3 j^2 \pi^2}\left(1 + \frac{a^2 u_2 \rho_0 k^2 I \cos 2\theta}{K_3 j^2 \pi^2 v^3}\right). \tag{12}$$

Likewise, suppose that the ultrasonic wave is suddenly switched off, so that the director relaxation occurs in an environment of $I=0$. The corresponding solution is

$$\beta_j(t) = \beta_j^{\mathrm{initial}} \exp\left(-t \Big/ \tau_j^{\mathrm{OFF}}\right) \tag{13}$$

with the off-time

$$\tau_j^{\mathrm{OFF}} = \frac{\gamma_1 a^2}{K_3 j^2 \pi^2}. \tag{14}$$

To compare the model with experiments, we must predict the optical intensity as a function of time. We can derive the optical intensity from our expression for the molecular tilt $\beta(z,\, t)$. For light propagating along the z-axis, perpendicular to the cell, the effective birefringence is

$$\begin{aligned} \Delta n_{\mathrm{eff}}[\beta(z,\, t)] &= \left(n_{\mathrm{e}}^{-2} \sin^2 \beta + n_{\mathrm{o}}^{-2} \cos^2 \beta\right)^{-1/2} - n_0 \\ &\approx \Delta n \sin^2 \beta. \end{aligned} \tag{15}$$

where n_{e} and n_{o} are the extraordinary and ordinary refractive indices of the liquid crystal, respectively, and $\Delta n = n_{\mathrm{e}} - n_{\mathrm{o}}$ is the birefringence of the material. We integrate the effective birefringence across the thickness of the cell to obtain the phase retardation

$$\delta(t) = \int_0^a \Delta n_{\mathrm{eff}}[\beta(z,\, t)]\,\mathrm{d}z \approx \frac{\pi a \Delta n}{\lambda} \sum_{j=1}^{\infty} \left[\beta_j(t)\right]^2 \tag{16}$$

where λ is the wavelength of the light. Hence, the optical intensity transmitted through crossed polarizers (for polarizers with optical axis 45° offset from the tilt plane) becomes

$$\begin{aligned} I_{\mathrm{opt}}(t) &= I_{\mathrm{min}} + I_0 \sin^2\left(\frac{\delta(t)}{2}\right) \\ &\approx I_{\mathrm{min}} + I_0 \sin^2\left\{\frac{\pi a \Delta n}{2\lambda} \sum_{j=1}^{\infty} \left[\beta_j(t)\right]^2\right\} \end{aligned} \tag{17}$$

where I_0 is the incoming optical intensity and I_{min} depends on the quality of the polarizers and of the liquid crystal surface alignment.

Note that the steady state Fourier modes β_j^{eq} should all scale linearly with low acoustic intensity I, with higher order corrections for larger I. For that reason, the steady state phase retardation δ should scale as I^2, and the steady state optical intensity as $\sin^2$ (constant I^2). In the experiment described below, the acoustic intensity I is proportional to V^2, where V is the voltage applied to the transducer. Hence, the steady state phase retardation δ should scale as V^4, and the steady state optical intensity as $\sin^2$ (constant V^4).

In this section, we have derived predictions for all of the Fourier modes $\beta_j(t)$. From these results, we see that the leading mode $j=1$ should dominate the rest. This mode has the largest steady state amplitude, 27 times larger than the next mode $j=3$ (to lowest order in acoustic intensity). It is also the slowest mode to relax, with on and off times 9 times slower than the next mode. Hence, we expect $j=1$ to be the only steady state or dynamic mode observable in the experiment.

As a final theoretical point, we can estimate numerical values for the on and off times. Equation (14) for the off-time is the classical prediction for the relaxation time of the Fréedericksz transition.

For the liquid crystal 5CB at room temperature of 25°C, the bend elastic constant is approximately $K_3 = 0.8 \times 10^{-11}$ N [15], and the rotational viscosity is approximately $\gamma_1 = 0.06$ Pa s [16]. For the cell thickness $a = 300\,\mu$m discussed below, we obtain $\tau_1^{OFF} = 70$ s.

In equation (12) for the on-time, the first term is the classical Fréedericksz relaxation time, while the second term is the leading correction, which shows how the on-time increases as a function of acoustic intensity. To estimate this increase, we use the following argument. By comparing equations (7) and (12), we see that the fractional increase in the on-time is

$$\frac{\Delta\tau_1^{ON}}{\tau_1^{ON}} = \frac{a^2 u_2 \rho_0 k^2 I \cos 2\theta}{K_3 j^2 \pi^2 v^3} = \frac{\beta_1^{eq}}{4 \tan 2\theta}. \qquad (18)$$

In a typical acousto-optic experiment, the acoustic intensity is increased up to the first peak in the steady state optical intensity. Equation (17) shows that this first peak occurs at the phase retardation $\delta^{eq} = \pi$, and hence at the tilt angle $\beta_1^{eq} = (\lambda/a\Delta n)^{1/2}$. In the experiment discussed below, we have $\lambda = 0.633\,\mu$m, $a = 300\,\mu$m, $\Delta n = 0.17$, and $\theta = 18°$. Hence, at the first peak, we expect the tilt angle to be $\beta_1^{eq} = 6°$, and the fractional increase in the on-time to be $\Delta\tau_1^{ON}/\tau_1^{ON} = 4\%$. This result shows that increasing acoustic intensity should cause the on-time to become slightly slower, but with the same order of magnitude.

3. Experiment

The acousto-optic response was measured for a commercially available room temperature nematic liquid crystal material, pentylcyanobiphenyl (5CB) (EM Industries). Cells were made with 2.5 inch × 2.5 inch plates of 900 μm thick Corning 1737 glass. A monolayer of octadecyltrichlorosilane (Gelest) was used to achieve homeotropic alignment. The cell was made with a liquid crystal layer thicknesses of 300 μm, determined by measuring the thickness of the cell at the centre using a micrometer and subtracting the thickness of each glass plate, to an accuracy of approximately 5 μm. This thickness was chosen because at much larger thicknesses, cell alignment becomes difficult. At lower thicknesses, the acousto-optic response is not significant within the applied acoustic intensity limits of the experiment. The cell was then sealed using an RTV compound for waterproofing.

A 75 gallon tank filled with de-ionized water was situated between crossed polarizers. The cell was suspended in the tank from a rotation stage. The acoustic wave was produced by a 1 inch immersion transducer (Santec Systems, Inc.), suspended from a second rotation stage in the tank 35 cm from the cell. The sinusoidal acoustic wave was generated by a Wavetek Model 90 function generator at 3.3 MHz. A 633 nm He:Ne laser beam was aligned with the acoustic spot and the change in optical intensity measured with a Newport Model 1830C optical power meter. All motion and data capture were computer-controlled using Labview.

As described previously [7, 8], our data were taken as follows. With the polarizers crossed, the optical axes of the molecules were first aligned along the direction of the laser beam. In the absence of an acoustic field, the cell was rotated around its polar axis (optical angle) and the angle of minimum optical intensity determined. This optical angle, θ_c, was then defined as zero. The optimum transducer angle $\theta_{t\ max} = 18°$ was determined by measuring the change in optical intensity at a fixed acoustic intensity over a range of transducer angles. Acousto-optic intensity as a function of time was measured. For each data set the final 100 data points were averaged to give an acousto-optic intensity. With the cell and transducer set at their respective optimum angles, the optical intensity as a function of applied acoustic intensity was then measured in the same way.

We previously reported the acoustic intensity based on the transducer calibration by the manufacturer, $I = 2.18\,V^2$, where I is the acoustic intensity in mW cm^{-2} received at the liquid crystal cell, and V is the peak-to-peak voltage applied to the transducer. A more recent calibration at our laboratory [17] indicates that the calibration is $I = 0.16\,V^2$, so that the acoustic intensity is lower and the liquid crystals are more sensitive than previously reported. Because the absolute acoustic intensity is not an issue for the current paper, we report our results here in terms of the peak-to-peak transducer voltage.

4. Results

For the 300 μm cell of 5CB, figure 2 shows a graph of the optical intensity as a function of the applied acoustic intensity, characterized by transducer voltage. Data are taken for 10 minutes, until a steady state is reached. The final 100 data points at each sound intensity are averaged to give the data points shown in the graph. With no applied acoustic field, the initial optical intensity is approximately 4 nW. As the acoustic intensity increases, the optical intensity increases until it reaches the first optical peak at 5 μW at a transducer voltage of 3.2 V. The steady state behaviour of this system has been discussed previously [7–9]. The following data relate to the dynamic behaviour of the liquid crystal cell, before the steady state is reached.

Figure 3 shows the dynamic behaviour of the system at two transducer voltages approaching the first optical

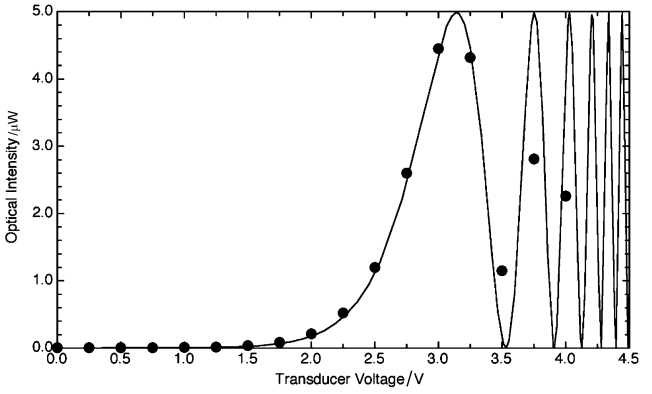

Figure 2. Steady state acousto-optic effect in a liquid crystal cell. The measured optical intensity is plotted as a function of the applied acoustic intensity, which is characterized by the voltage applied to the transducer.

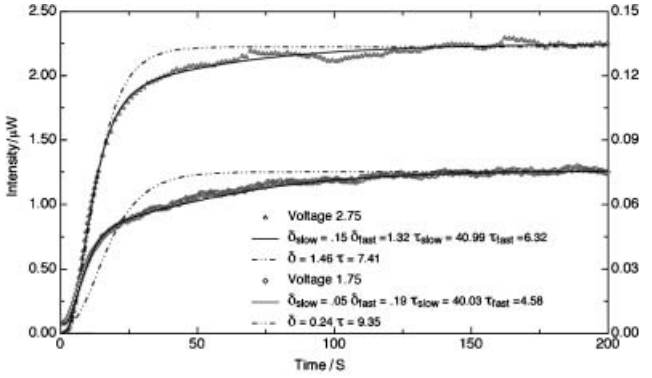

Figure 3. Optical intensity as a function of time after an ultrasonic wave is applied to the liquid crystal cell. Lower plot: transducer voltage of 1.75 V, see optical intensity axis on the right. Upper plot: transducer voltage of 2.75 V, see optical intensity axis on the left. In each case, the dot-dashed curve shows the fit to a single-exponential process, and the solid curve shows the double-exponential fit.

peak, 1.75 and 2.75 V. In each case, the optical intensity is measured every 250 ms for a period of 10 min, although the figure only shows the behaviour for the first 3 min. The acoustic intensity is applied at the time $t=0$, and held constant for the length of the scan. The optical intensity increases to the steady state value within approximately 50 s in both cases.

To analyse the results quantitatively, the data in figure 3 are fit with a single exponential process describing the leading relaxation mode, based on the dynamics predicted in § 2. The specific fitting function, derived from equations (11) and (17), is

$$I_{\mathrm{opt}}(t) = I_{\mathrm{min}} + I_0 \sin^2\left\{\frac{1}{2}\delta[1-\exp(-t/\tau)]^2\right\} \quad (19)$$

where we drop the labels from δ^{eq} and $\tau_1{}^{\mathrm{ON}}$ for compactness. The parameters I_{min} and I_0 are fixed from the steady state data, so that δ and τ are the only dynamic fitting parameters. Surprisingly, this single-exponential process gives unsatisfactory fits to the data, as shown by the dashed lines in the figure. The fit captures the initial rapid increase in the optical intensity, and it saturates at the right level, but it cannot describe the dynamic change in slope of the optical intensity over the intermediate range of time. This discrepancy is more severe at the lower voltage of 1.75 V, but is also seen at the higher voltage of 2.75 V.

Because the single-exponential fits are unsatisfactory, we must consider the possibility that the system has two distinct relaxation modes with different time scales. This could occur, for example, if one of the higher order Fourier modes in the tilt profile has an anomalously high amplitude, so that it contributes significantly to the dynamics. To model a process with two relaxation modes, we use the double-exponential fitting function

$$I_{\mathrm{opt}}(t) = I_{\mathrm{min}} + I_0 \sin^2\left\{\frac{1}{2}\delta_{\mathrm{fast}}\left[1-\exp\left(-t/\tau_{\mathrm{fast}}\right)\right]^2 + \frac{1}{2}\delta_{\mathrm{slow}}\left[1-\exp\left(-t/\tau_{\mathrm{slow}}\right)\right]^2\right\} \quad (20)$$

The double-exponential fits are shown by the solid lines in figure 3. Clearly these fits are much better than the single-exponential fits, as they pass through the data for early, intermediate, and late time regimes. This improvement is most dramatic for the lower transducer voltage of 1.75 V, but is also noticeable at 2.75 V.

For comparison, we also attempt to fit the data to the stretched exponential function $I_{\mathrm{opt}}(t) = I_{\mathrm{min}} + I_0 \sin^2\left\{\frac{1}{2}\delta[1-\exp(-(t/\tau)^{\nu})]^2\right\}$, where ν is a fractional exponent. However, the fits are distinctly worse than the double-exponential, so we do not consider this fitting approach further.

Additional dynamic data for other acousto-optic scans are shown in figures 4 and 5. In figure 4, the transducer voltages range from the low level of 2.25 V up to an intensity near the first optical peak (3.25 V). In all of these cases, the double-exponential function gives good fits to the dynamic behaviour over the full range of time. By contrast, the single-exponential fits (not shown) are unsatisfactory, with the worst discrepancies at the lowest transducer voltages.

In figure 5, the transducer voltages extend well past the first optical peak. At 3.5 V, between the first and second optical peaks, the double-exponential fit agrees very well with the data, as the optical intensity passes through a peak and then decreases to the steady state level. At the higher transducer voltages, a new discrepancy is seen between the fit and the data: the fit shows the optical intensity oscillating between 0 and

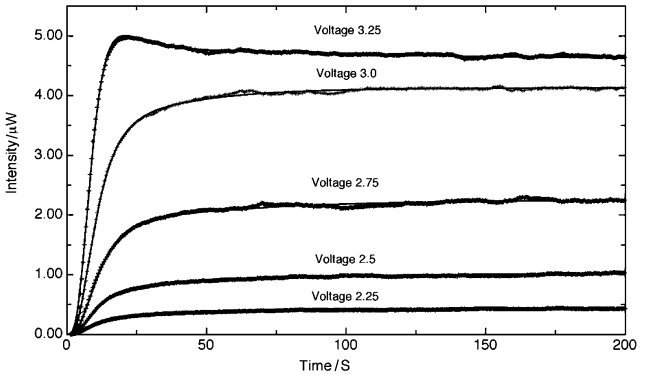

Figure 4. Optical intensity as a function of time for several acoustic intensities up to the first optical peak. The solid lines show good fits to a double-exponential process in all cases.

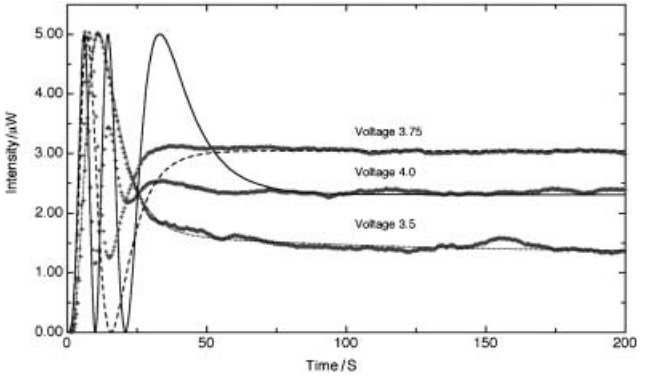

Figure 5. Optical intensity as a function of time for three acoustic intensities beyond the first optical peak. The lines show a good fit to a double-exponential process for 3.5 V, which is between the first and second optical peaks. For higher voltages, the data differ from the prediction, in that the oscillations in optical intensity are damped out.

5 μW, while the experimental variation is damped out. This damping is similar to the behaviour in the steady state data of figure 2 beyond the first optical peak. We attribute this damping to a non-uniform sound intensity over the region of liquid crystal probed by the experiment, which leads to an optical intensity that averages over peaks and valleys. Because of this behaviour, we only report data up to 3.5 V in the analysis below.

In addition to these results for the dynamic behaviour after the ultrasonic wave is switched on, we also investigate the relaxation process after the ultrasonic wave is switched off. A typical example is presented in figure 6, for switching off from a transducer voltage of 2.75 V. The main plot shows the full dynamic behaviour, while the inset shows details of the region where

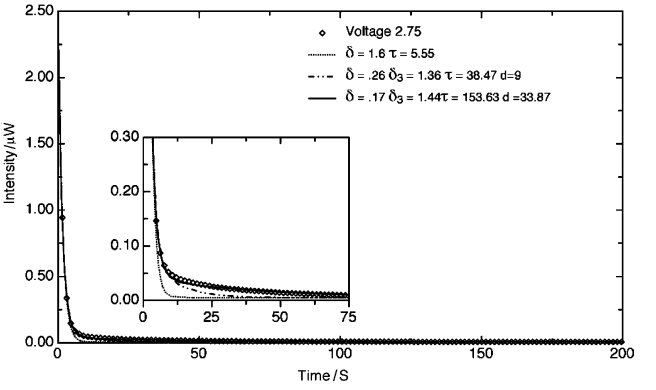

Figure 6. Optical intensity as a function of time after an ultrasonic wave with transducer voltage of 2.75 V is turned off. The inset shows details of the region where the significant slope change occurs. The curves show fits to a single-exponential process (dotted line), a double-exponential process with $\tau_{slow}/\tau_{fast}=9$ (dot-dashed line), and a double-exponential process with $\tau_{slow}/\tau_{fast}=34$ (solid line).

the significant slope change occurs. The results are modelled with the single-exponential fitting function

$$I_{opt}(t) = I_{min} + I_0 \sin^2\left[\frac{1}{2}\delta \exp\left(-2t/\tau\right)\right] \qquad (21)$$

as shown by the dotted line, but this fit suffers from the same problems seen in the single-exponential fits of the switching-on behaviour. For that reason, we consider the double-exponential decay function

$$I_{opt}(t) = I_{min} + I_0 \sin^2\left[\frac{1}{2}\delta_{fast} \exp\left(-2t/\tau_{fast}\right) + \frac{1}{2}\delta_{slow} \exp\left(-2t/\tau_{slow}\right)\right] \qquad (22)$$

We first fit the data using the constraint $\tau_{slow}/\tau_{fast}=9$, as found for the on-times, giving the dot-dashed line. This fit is an improvement over the single-exponential fit, but is still not consistent with all of the data. Hence, we remove this constraint and allow τ_{slow} and τ_{fast} to be independent parameters. In this case, the double-exponential fit passes through the data for early, intermediate and late time regimes, and the ratio of the two time scales is approximately 34.

Further results for the dynamic relaxation process are shown in figure 7. In this plot we see the change in optical intensity after the ultrasonic wave is turned off from various initial transducer voltages. The values of the initial transducer voltage range from 2 to 3.5 V, which is just above the voltage required to reach the first optical peak. In all cases, the unconstrained double-exponential function fits the data very well. Again the single-exponential fits (not shown) are

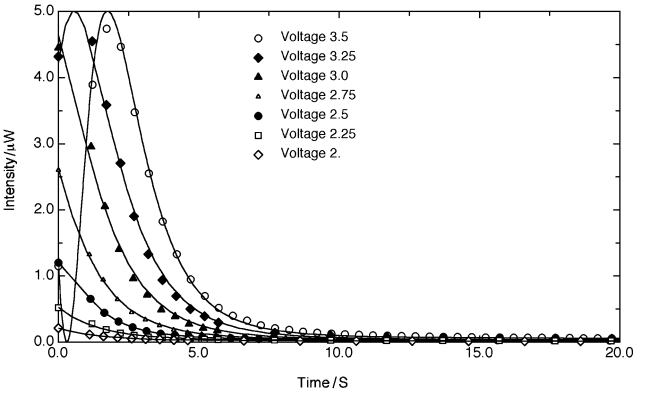

Figure 7. Optical intensity as a function of time after an ultrasonic wave is turned off, for several initial acoustic intensities.

inconsistent with the data in the intermediate time regime.

To summarize the ensemble of fit results, figures 8 and 9 show the on- and off-times as functions of applied voltage. The on-time for the fast mode, shown in figure 8, begins at approximately 5 s for the lowest detectable acoustic intensity, and increases to approximately 7 s around the first optical peak. The on-time for the slow mode in figure 9 increases from 45 to 60 s over the same range of applied voltage. The ratio between these two time scales is approximately a constant factor of 9.

The off-time for the fast mode remains approximately constant at 5 s from the lowest transducer voltage up to a transducer voltage around the first optical peak. This off-time agrees with the low voltage limit of the fast mode on-time. The off-time for the slow mode is scattered from 150 to 180 s with no discernable trend as a function of applied voltage. The ratio between these

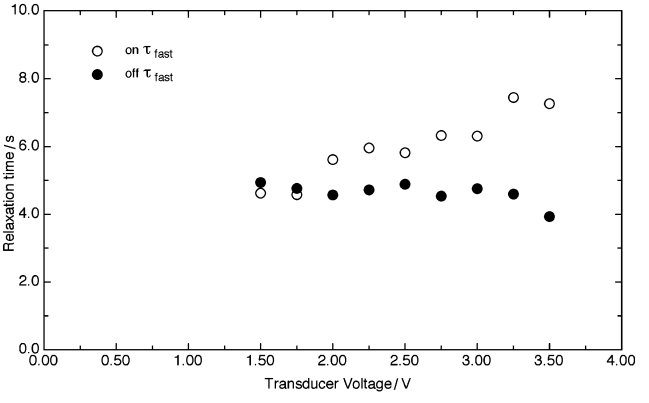

Figure 8. Relaxation time for the fast mode as a function of transducer voltage, for both switching-on and switching-off processes.

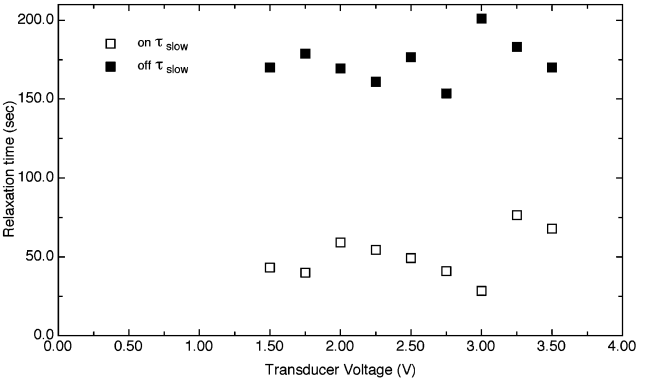

Figure 9. Relaxation time for the slow mode as a function of transducer voltage, for both switching-on and switching-off processes.

two time scales is approximately a constant factor of 33 ± 3.

Figure 10 shows the corresponding results for the amplitudes δ_{fast} and δ_{slow} of the two relaxation modes versus the applied voltage, plotted on a log–log scale. Note that the fit results for these two amplitudes are consistent between the switching-on and switching-off processes. This consistency is significant, because it shows that our fitting procedure identifies the same two modes for switching-on and switching-off, even though the slow time scales are different for these two processes.

The two amplitudes δ_{fast} and δ_{slow} have very different behaviour as functions of transducer voltage. The log–log plot shows clearly that these amplitudes follow power laws with significantly different exponents:

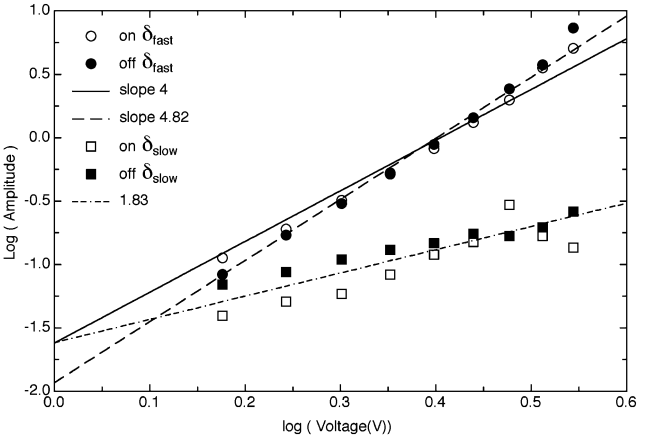

Figure 10. Amplitudes of the fast and slow modes as functions of transducer voltage, plotted on a log–log scale, for both switching-on and switching-off processes. The power law fit for the fast mode shows an optimum exponent of 4.82 (dashed line), which is close to the theoretically predicted exponent of 4 (solid line). The power law fit for the slow mode shows an optimum exponent of 1.83 (dot-dashed line).

δ_{fast} scales approximately as V^4, while δ_{slow} scales approximately as V^2. As a result, the two modes have comparable amplitudes at low voltage, but the fast mode dominates at higher voltages. This behaviour explains why the quality of the single-exponential fit is worst at low voltage.

5. Discussion

In the previous section, we presented an experimental study of the dynamics of the acousto-optic effect after an ultrasonic wave is switched on or off. This study showed that there are two relaxation modes: a fast mode with a relaxation time of approximately 5–7 s (switching-on or -off) and a slow mode with a relaxation time of approximately 45–60 s (switching-on) or 150–180 s (switching-off). At this point, a key question is how to compare these experimental results with the Fréedericksz-type theory in § 2. In particular, do either or both of these modes correspond to the dynamic modes predicted theoretically?

Because the theory predicts a series of Fourier modes, each with its own relaxation time, one might speculate that the two observed modes could correspond to two distinct Fourier modes, probably the leading two modes $j=1$ and $j=3$. This speculation is supported by the fact that the ratio of relaxation times $\tau_{slow}/\tau_{fast}=9$ for the *switching-on* process, which agrees with the prediction of equation (12) (in the limit of low acoustic intensity I) for $j=1$ and 3. However, there are two problems with this speculation. First, for the *switching-off* process, the ratio of relaxation times is approximately 33. This ratio is quite far from the predicted value of 9 for the leading two modes. Second, our fits show that the slow mode amplitude δ_{slow} is generally less than the fast mode amplitude δ_{fast}. This result does not fit the theoretical prediction that the slowest Fourier mode $j=1$ should have a much greater amplitude than the second-slowest Fourier mode $j=3$. For these reasons, we cannot associate the two observed modes with the predicted Fourier modes $j=1$ and $j=3$.

Since the observed pair of modes is not consistent with the predictions for $j=1$ and $j=3$, the next question is: do *either* of the modes fit the predicted dynamics? Our results show that the observed fast mode is consistent with the theory, while the observed slow mode has a different type of behaviour. First, the amplitude of the fast mode scales with transducer voltage V approximately as $\delta_{fast} \propto V^4$, and hence with acoustic intensity I as $\delta_{fast} \propto I^2$, in agreement with the prediction of equations (7) and (16). By comparison, the amplitude of the slow mode scales approximately as $\delta_{slow} \propto V^2$, and hence as $\delta_{slow} \propto I$. Further evidence comes from the behaviour of the on- and off-times. For the fast mode, the on-time depends on acoustic intensity, while the off-time is approximately equal to the zero-intensity limit of the on-time, in agreement with the prediction of equations (12) and (14). By comparison, for the slow mode, the off-time is more than 3 times longer than the on-time.

For an additional test of the theory, we can compare the numerical estimates at the end of § 2 with the observed on- and off-times for the fast mode. For the cell thickness $a=300\,\mu m$, bend elastic constant $K_3=0.8\times10^{-11}\,N$ [15], and rotational viscosity $\gamma_1=0.06\,Pa\,s$ [16], the theory predicts the off time $\tau_1^{OFF}=70\,s$ for the dominant ($j=1$) mode. This is about an order of magnitude larger than the observed off time of 5 s. The discrepancy may be caused by uncertainty in the parameters K_3 and γ_1, which are both quite sensitive to temperature changes of a few degrees around 25°C. Alternatively, it may be caused by chemical impurities in the sample. The theory also predicts that the on-time should increase linearly with acoustic intensity, with a fractional increase of approximately 4% from zero acoustic intensity to the first optical peak. The observed on time also increases approximately linearly with acoustic intensity, although the fractional increase from zero to the first optical peak is closer to 50%. This difference is probably related to the lowest order expansion in powers of the acoustic intensity, and could be fit by a higher order power series.

If the observed fast mode is the dominant mode predicted by the Fréedericksz-type theory, what is the observed slow mode? We do not yet have a model for this mode, but can make some speculations. This mode must involve features of the acoustic realignment of nematic liquid crystals which do not occur in the Fréedericksz transition induced by an electric or magnetic field. One key feature of acoustics is that ultrasound can form standing wave patterns within a cell, leading to nodes and antinodes in the acoustic intensity. Such standing wave patterns lead to peaks in the acousto-optic effect when the frequency and incident angle of the ultrasound come into resonance with the thicknesses of the liquid crystal and the glass walls. In previous publications, we have investigated these resonances experimentally [8] and theoretically [9].

Liquid crystal molecules may interact with the standing wave pattern by flowing toward or away from the nodes or antinodes. This flow of molecules would be a slow effect, quite different from molecular rotation, and it would come to equilibrium on a different time scale. Furthermore, this flow could have different relaxation times when ultrasound is turned on or off.

Although this non-uniform flow effect is not described by our current theory, the experimental results show that it should be an important extension of the theory. We are currently working on molecular dynamics simulations of ultrasonic waves acting on liquid crystals, and these simulations may help to elucidate this issue.

Regardless of the fundamental origin of the slow mode, our experimental results show the type of dynamic behaviour that can be expected in technological devices using the acousto-optic effect. In such devices, there will be two distinct dynamic modes when an ultrasonic wave is switched on or off: a dominant fast mode that reaches a steady state in a few seconds, and a lower amplitude slow mode that extends over a much longer time scale. For acoustic imaging applications, it will be important to design devices that produce an image from the fast mode and do not wait for the slow mode.

In conclusion, we have presented a theoretical and experimental study of the dynamics of the acousto-optic effect in a nematic liquid crystal. Our experiments show that the system has two modes of relaxation, characterized by different time scales and different dependences on acoustic intensity. The fast mode is qualitatively consistent with our Fréedericksz-type theory, but the slow mode exhibits a novel behaviour associated with the acoustic realignment of a liquid crystal.

Acknowledgments

We would like to thank B. Houston, R. Corsaro, and H. Simpson for helpful discussions. This work was supported by the Office of Naval Research and the Naval Research Laboratory.

References

[1] S. Candau, S.V. Letcher. In *Advances in Liquid Crystals*, G.H. Brown (Ed.), pp. 167–235, Academic, New York (1978).
[2] O.A. Kapustina. In *Physical Properties of Liquid Crystals*, D. Demus, J.W. Goodby, G.W. Gray, H. Spiess (Eds), pp. 549–568, Wiley-VCH (1999).
[3] J.-L. Dion. *C. R. Acad. Sc. Paris*, **284**, 219 (1997); J.-L. Dion and A.D. Jacob. *Appl. Phys. Lett*., **31**, 490 (1977); J.-L. Dion. *C. R. Acad. Sc. Paris*, **286**, 383 (1978); J.-L. Dion. *J. appl. Phys*., **50**, 2965 (1979); J.-L., Dion, R. Simard, A.D. Jacob and A. Leblanc. *Ultrasonics Symposium*, pp. 56–59, IEEE, New York (1979).
[4] J.S. Sandhu, W.J. Popek, H. Wang. U.S. Patent No. 5,796,003 (1998); J.S. Sandhu, W.J. Popek and H. Wang. U.S. Patent 6 049 411 (2000).
[5] D.W. Gerdt, M.C. Baruch, C.M. Adkins. *Proc. SPIE*, **3635**, 58 (1999).
[6] J.S. Sandhu, H. Wang, W.J. Popek. *Proc. SPIE*, **3955**, 94 (2000).
[7] J.V. Selinger, M.S. Spector, V.A. Greanya, B.T. Weslowski, D.K. Shenoy, R. Shashidhar. *Phys. Rev. E*, **66**, 051708 (2002).
[8] V.A. Greanya, M.S. Spector, J.V. Selinger, B.T. Weslowski, R. Shashidhar. *J. appl. Phys.*, **94**, 7571 (2003).
[9] A.P. Malanoski, V.A. Greanya, B.T. Weslowski, M.S. Spector, J.V. Selinger, R. Shashidhar. *Phys. Rev. E*, **69**, 021705 (2004).
[10] F. Bonetto, E. Anoardo, R. Kimmich. *Chem. Phys. Lett.*, **361**, 237 (2002).
[11] F. Bonetto, E. Anoardo, R. Kimmich. *J. chem. Phys.*, **118**, 9037 (2003).
[12] F. Bonetto, E. Anoardo. *Phys. Rev. E*, **68**, 021703 (2003).
[13] P. Pieranski, F. Brochard, E. Guyon. *J. Phys. (Paris)*, **34**, 35 (1973).
[14] I.W. Stewart. *The Static and Dynamic Continuum Theory of Liquid Crystals,* §3.4 and 5.9, Taylor & Francis, London (2004).
[15] A. Bogi, S. Faetti. *Liq. Cryst.*, **28**, 729 (2001).
[16] A. Raviol, W. Stille, G. Strobl. *J. chem. Phys.*, **103**, 3788 (1995).
[17] H. Simpson. Private communication (2004).